applied optics

Behaviors of photovoltaic cells illuminated by a laser of different operation modes

Rui-Ting Chang,[1,2] Cong Liu,[1,2] Chen-Guang Huang,[2] and Chen-Wu Wu[1,*]

[1]Institute of Mechanics, Chinese Academy of Sciences, Beijing, 100190, China
[2]School of Engineering Science, University of Chinese Academy of Sciences, Beijing, 100049, China
*Corresponding author: chenwuwu@imech.ac.cn

Received 4 April 2022; revised 7 June 2022; accepted 11 June 2022; posted 14 June 2022; published 27 June 2022

The ultimate capability of light-electricity conversion of a laser with different operation modes in a typical photovoltaic (PV) cell was investigated for the technologic concept of laser power transmission (LPT). The quasi-linear correlation between the maximum allowable laser power density and the pulsed laser power percentage (*PPP*) of the combined dual lasers was found experimentally on a tri-junction GaAs PV cell. At the same time, the patterns of thermomechanical damage in the PV cells were characterized. The physical mechanism on the difference in the light-electricity conversion ability for a multi-pulse (MP) laser and a continuous wave (CW) laser was revealed by the coupled model on thermal diffusion and the carrier transport.

https://doi.org/10.1364/AO.460270

1. INTRODUCTION

Laser power beaming (LPB) has been convincing as a promising power supply technology, in particular when applied to support efficient light-electricity conversion with photovoltaic (PV) cells for long-distance power transmission [1,2]. The concepts of laser powered mobile phones, wireless sensors, and drones [3,4] have been extensively demonstrated by several research groups. A typical system of LPB is fundamentally composed of a transmitter and a receiver, for which a PV cell panel is always adopted in the receiver to realize the procedures of light-electricity conversion. Therefore, the actual light-electricity conversion efficiency and capacity of the PV cell of laser energy play a crucial role in the technology of LPB [5].

As has been reported, the actual light-electricity conversion efficiency of the PV cells will decrease with an increase of the laser power density [2,6–8]. From the point of view of thermodynamics, the output electrical power decreases with the increase of the input laser energy density [9–11] when the latter reaches a certain threshold, which is determined by the coupling competition between light-electricity conversion and light-heat dissipation [8,12], although the maximum useful power will rise to a higher level if we presciently regulate the equilibrium temperature for a given assembly scheme and thermal-mechanical boundary conditions [12]. Otherwise, the PV cell will also be distorted and damaged by the excessive thermal stress [10,12–14], which finally leads to the permanent failure of the PV cell. From a microscopical perspective, increasing the input laser energy density will raise the carrier concentration in PV cells, which would enhance carrier diffusion mobility and recombination rate simultaneously [15,16], which will lead to complicated effects on the light-electricity conversion efficiency.

Therefore, it is important to find an optimized spatiotemporal distribution of input laser energy to maximize the light-electricity conversion capability [17–19], on which some novel attempts on altering the laser operation modes are worthwhile. This could be realized via adopting both the continuous wave (CW) laser and the multi-pulse (MP) laser with tailorable peak power, duty ratio, and repetition frequency. The present work first proposed such strategy as applying the combined CW laser and MP laser in light-electricity conversion and then investigated the electrical/thermal responses of a typical PV cell to the combined illumination by the CW laser and MP laser. Finally, we established the coupled model on carrier transportation and thermal diffusion to reveal the mechanism on the experimental phenomenon.

2. EXPERIMENTAL

Figure 1 exhibits the tri-junction GaAs/GaInP/Ge PV cells [19,20] and experimental setup to examine the responses of the PV cell to illumination by the combined CW and MP lasers. Note that the wavelength of both lasers is 808 nm, and the pulse duration and the repetition frequency of the MP laser are 45 μs and 3 kHz, respectively. Moreover, the degree of mixture in the power of the MP laser and CW laser is defined as so-called power percentage of the pulsed laser (*PPP*), which is the ratio of the average power density of the MP laser to the total power density. The open-circuit (OC) voltage and temperature of the PV cell are measured by the voltmeter and thermocouple, respectively. The central control computer is used to control the laser parameters and record the real-time voltage and temperature data. The possible effects of joule heating since the external electrical load

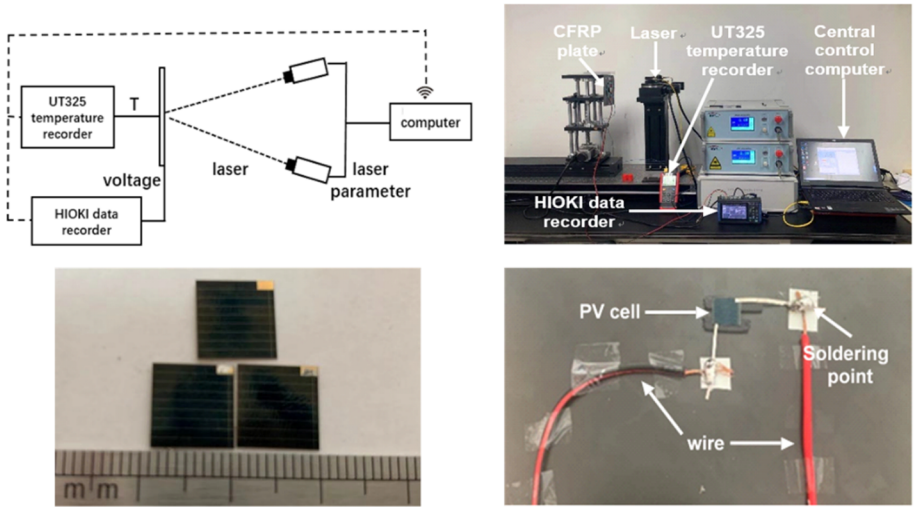

Fig. 1. PV cells and setup.

could be restrained via distant placing and OC voltage or short circuit current could be largely utilized to further suppress such deviations.

Optical microscopy (OM) and scanning electron microscopy (SEM) were used to observe the microscopic morphology of the failed PV cells as shown in Fig. 2. The surface morphology of the failed PV cells indicates that the damage in the PV cells is mainly manifested as quasi-transparent bubbles, of which the characteristic of Gaussian distribution conforms to that of the laser energy distribution. Two typical damage patterns in PV cells, one corresponding to the test by only the CW laser and the other by the combined CW/MP laser ($PPP = 75\%$), were further observed by OM, as shown in Figs. 2(b) and 2(c), respectively. It is indicated that the high proportion of the MP laser in illumination would lead to more evenly scattered dotted regions, which is especially obvious when compared with the cases with only the CW laser.

The damage evolution in the PV cells is schematically described in Figs. 1(d)–1(f) with the mixture degree $PPP = 77\%$. At the very beginning, a thin torus with an average diameter of about 60–120 μm appears with a small bright aperture [Fig. 2(d)]. Then, the aperture grows up along the torus and thicken the torus [Fig. 2(e)]. Later, more interface separation arises to form a set of tori [Fig. 2(f)], in which the different colors demonstrate the different statuses of interface damage. After that, the interface separation gradually becomes larger and larger, and finally, the top layer material fractures and peels off when the thermal stress is high enough. Such similar procedures would be repeated within the illuminated region in the PV cells.

The above typical damage characteristics are further revealed by SEM as shown in Figs. 2(g)–2(i) with $PPP = 75\%$. It is verified again in Figs. 2(g) and 2(h) that the generation of small bubbles is mainly caused by the interfacial separation of the PV cell material, and some electrode material was obviously melted. These features might have been due to the complex interaction between the defect induced surface-plasmon polaritons and the incident MP laser that resulted in a spatially modulated deposition of the MP laser energy. The "bubble-like" damage was further magnified as in Fig. 2(i) to reveal the snowflake-like

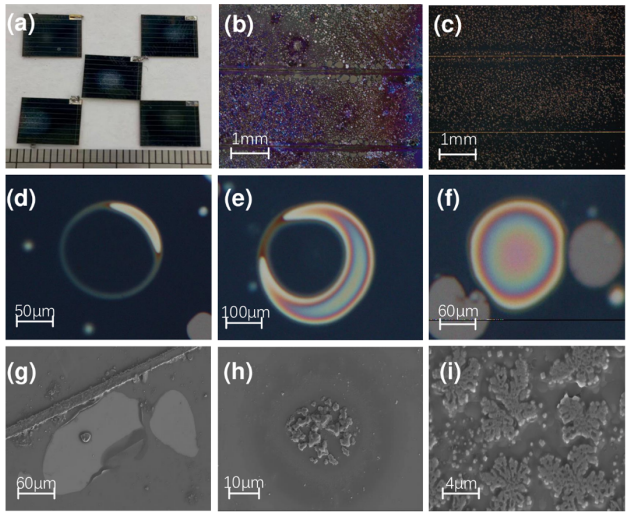

Fig. 2. (a) PV cells after test; (b) OM morphology of cell illuminated by CW laser; (c) OM morphology of cell illuminated by MP laser; (d)–(f) damage evolution in cells; (g)–(i) SEM morphology of cells illuminated by the combined CW/MP laser.

microscopical structure in the resolidified material of failed PV cells.

The failure criterion of the PV cell is, therefore, defined by its OC voltage dropping to be lower than 20% of that of the intact PV cell when the temperature of the illuminated PV cell returns to the room temperature after removing the laser, for which the total illumination timespan is approximately 10 s. Figure 3 illustrates the critical points, i.e., the maximum permitted input laser power density upon the PV cells for a set of cases with different mixture degrees of the combined lasers, i.e., different value of *PPP*. That is to say, the PV cell would fail if it was subjected to the illumination by the combined laser of power density beyond the critical points. In detail, the magnitude of *PPP* is written immediately below the sequence number of every case, and the error bar is given with the tangent of its inclination angle being [*PPP*/(1-*PPP*)], which means that the error bar will be steeper for larger *PPP*. It is revealed in Fig. 2

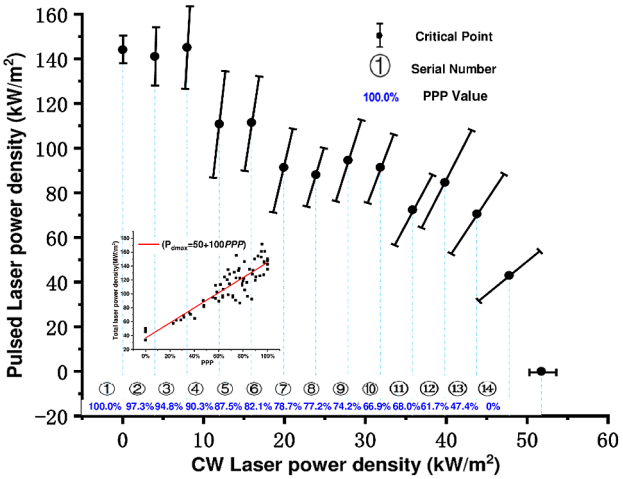

Fig. 3. Critical power density for the hybrid laser of different mixture degrees.

that the failure threshold of power density to the present PV cell is approximately 145 kW/m^2 when $PPP = 1$ and 52 kW/m^2 when $PPP = 0$, respectively. Empirically, the empirical formula correlating the maximum permitted power density with PPP is obtained as

$$P_{\mathrm{dmax}} = 1000 \times (0.052 + 0.093PPP) \approx 50 + 100PPP, \quad \textbf{(1)}$$

wherein the maximum permitted power density P_{dmax} of unit kW/m^2 includes the contribution of both the MP laser and CW laser, which implies that the critical total power density will decrease with increasing the proportion of the CW laser.

The competition between thermodynamic dissipation and light-electric conversion [2,8] in the PV cells illuminated by the combined dual laser was studied, with the OC voltage and cell temperature versus input laser power density being measured and analyzed for sets of tests. The time history of the relative temperature elevation ($\Delta T/T_0$) and OC voltage variation ($\Delta U/U_0$) under illumination are shown in Figs. 4(a) and Fig. 4(b), respectively. Note that T_0 and U_0 represents the ambient temperature and the initial OC voltage of the GaAs PV cell, respectively. The sequence number in Fig. 4 might not exactly correspond to the sequence numbers in Fig. 3, although all the data of the former was extracted from the latter.

It can be found in Fig. 4 that both $\Delta T/T_0$ and $\Delta U/U_0$ are positively correlated with the total laser energy density. The data sets numbered as 5, 6, and 9 of the test cases with same total laser power density representing the relative temperature increment and voltage increment were compared in Figs. 4(c) and 4(d), respectively. It is shown that temperature of the PV cell decreases while its peak OC voltage increases with increasing PPP, which means that the actual light-electricity conversion efficiency of the PV cell would increase with increasing PPP. This could be due to the differences in thermodynamic dissipation and thermal diffusion, as well as carrier transportation in the PV cells illuminated by the MP laser and CW laser.

3. THEORETICAL

The absorbed laser energy by the PV cell would change into electrical energy via carrier excitation and collection as well as thermal energy due to carrier recombination and bremsstrahlung, in which the latter results from the redundant kinetic energy of the incident photon in excess of the bandgap. The thermal energy accumulation means elevated temperature of the PV cell that could decrease the probability of carrier collection and, therefore, increase thermal dissipation, which is obviously a coupled competition from the point of view of energy [8]. Such competition could be described by the coupled equations of both carrier transportation and thermal diffusion.

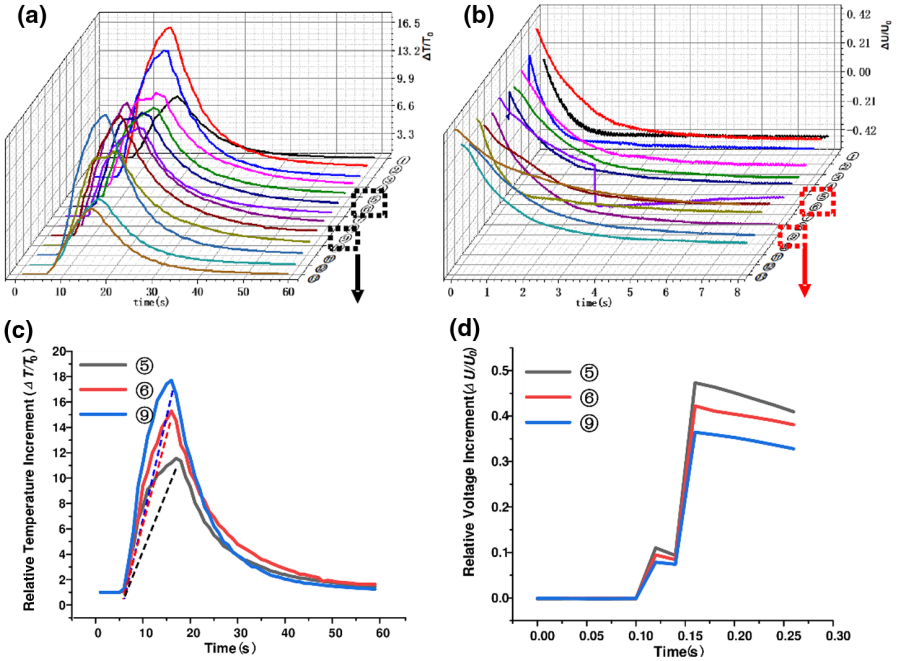

Fig. 4. Time history of (a) temperature variation ($\Delta T/T_0$), (b) voltage variation ($\Delta U/U_0$), magnified parts of (c) ($\Delta T/T_0$) and (d) ($\Delta U/U_0$).

The two-dimensional equation governing carrier transportation [20] in the region segmented by the two adjacent electrode grids in a PV cell under laser illumination could be expressed as Eq. (2) for any state of specified temperature,

$$\frac{\partial \mathrm{n}}{\partial t} = D\nabla^2 n + \mu \nabla n \cdot E - \frac{n}{\tau} + G, \tag{2}$$

with boundary conditions $n = 0$ upon the edges connected to the electrodes. Herein, n is the carrier density, D is the diffusional coefficient, E is the built-in electric field strength, τ is the carrier lifetime, and operator $\nabla = (\partial/\partial x, \partial/\partial y)$. The carrier generation rate G is determined by the quantum efficiency γ, intensity of laser I, laser frequency ν, and Planck's constant h, as expressed in Eq. (3),

$$G = \frac{\gamma I}{h\nu}. \tag{3}$$

The temperature-dependent drift coefficient μ [20] could be approximated as

$$\mu = \mu_0 (T_0/T)^2. \tag{4}$$

Also, we have the Einstein relation [19] as

$$D = kT\mu/q, \tag{5}$$

with q being the electric charge of the carrier.

The light-to-electric conversion efficiency could be approximated by the ratio of carrier collection rate upon the electrode to the carrier excitation rate by the laser. The carrier collection rate is equivalent to the theoretical current J that includes drifting current J_1 and diffusing current J_2 [20] defined by Eqs. (6) and (7), a pure counting procedure without distinguishing the electron and hole,

$$J_1 = q\mu n E, \tag{6}$$

$$J_2 = qD\frac{\partial n}{\partial x}. \tag{7}$$

Therefore, the theoretical current J and carrier collection rate N could be obtained [20] as Eqs. (8) and (9),

$$J = J_1 + J_2 = q\mu n E + qD\frac{\partial n}{\partial x}, \tag{8}$$

$$N = \frac{J}{q} = \mu n E + D\frac{\partial n}{\partial x}. \tag{9}$$

Then, the light-to-electric conversion efficiency η could be derived as Eq. (10) and the light-to-heat conversion percentage as $(1-\eta)$,

$$\eta = \frac{\int N dt \cdot E_g}{\int g_p \mathrm{d}t} \times 100\%, \tag{10}$$

wherein the bandgap E_g in a multi-junction PV cell is approximated by the weighted average of all the junction materials participating in the PV effect.

The one-dimensional equation of T governing the thermal diffusion [2,8,21] could be adopted as Eq. (11) because the PV cell depth is extremely small in comparison with its width,

Table 1. Geometrical and Physical Parameters [8,9,12,20]

Parameter	Unit	Magnitude
l	[m]	1.00×10^{-3}
d	[m]	3.00×10^{-5}
a	[m]	1.00×10^{-4}
γ	[1]	0.80
r	[m]	5.00×10^{-3}
I	$[\mathrm{W \cdot m^{-3}}]$	7.49×10^{8}
		1.01×10^{8}
h	$[\mathrm{J \cdot s}]$	6.63×10^{-34}
v	$[\mathrm{s^{-1}}]$	3.70×10^{14}
T_0	[K]	3.00×10^{2}
μ_0	$[\mathrm{m^2 \cdot V^{-1} \cdot s^{-1}}]$	0.80
E	$[\mathrm{V \cdot m^{-1}}]$	2.18×10^{2},
		3.74×10^{2}
k	$[\mathrm{J \cdot K^{-1}}]$	1.38×10^{-23}
q	[c]	1.60×10^{-19}
Eg (GaInP)	[eV]	1.81
Eg (GaAs)	[eV]	1.42
Eg (Ge)	[eV]	0.67
τ	[s]	1.00×10^{-7}
k_c	$[\mathrm{W \cdot m^{-2} \cdot K^{-1}}]$	1.30×10^{2}
ρ	$[\mathrm{kg \cdot m^{-3}}]$	2.33×10^{3}
C	$[\mathrm{J \cdot kg^{-1} \cdot K^{-1}}]$	7.00×10^{2}

$$\rho C\frac{\partial T}{\partial t} = k_c\frac{\partial^2 T}{\partial x^2} + I(1-\eta). \tag{11}$$

With boundary conditions of natural convective heat transfer and thermal radiation to ambient being applied [2,8,10,12,21], wherein k_c is heat thermal conductivity, ρ is density, and C is specific heat capacity, for which the weighted averages of the physical parameters of the main materials in the PV cell are utilized. Therefore, the carrier transportation and thermal diffusion are intrinsically coupled via Eqs. (2)–(11), which should be solved simultaneously.

The geometrical and physical parameters used in the calculation are listed in Table 1 for the multi-junction GaAs PV cells illuminated by the combined laser of different *PPP*. The sketches of the computational domain, typical carrier concentration fields, thermal dissipation percentages versus temperature, and relative temperature increment versus time are plotted in Figs. 5(a)–5(d).

As shown in Fig. 5(a), the two-dimensional cross section of the PV cell sectioned by two adjacent strip electrodes is taken as the computational domain considering the spatial periodicity of the cell structure, in which "a" represents half-width of the edge covered by the electrode, "d" represents the total junction thickness, and "l" represents the center distance of two adjacent electrodes.

The carrier density fields in the PV cell at several instances are shown in Fig. 5(b), which indicates a uniform distribution of carriers in the PV cell at the very beginning with an extreme steep density gradient around the electrode. A steady density field would be achieved in less than 1 μs driven by the large density gradient sustained by the electrode that collects the carriers.

Figure 5(c) plots the calculated thermal dissipation percentages versus temperature for the cases with the MP laser and CW

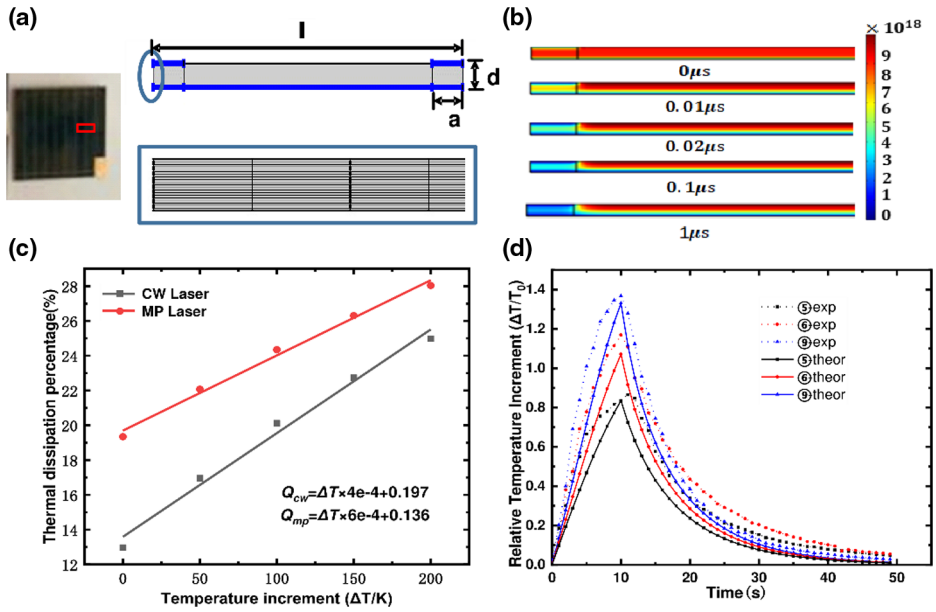

Fig. 5. (a) Sketch of the geometry and computational domain, (b) typical contours of carrier density, (c) thermal dissipation percentages versus temperature, and (d) relative temperature increment ($\Delta T/T_0$) of the PV cell for the cases of different *PPP*.

laser, which implies good linearity in the trend lines for both cases of the MP laser and CW laser. It is also shown that thermal dissipation in the PV cell under MP laser illumination is lower than that of CW laser. However, such a difference in thermal dissipation would be smaller and smaller with the temperature rising, and it is imaginable that more MP laser energy would dissipate into heat when compared with the cases of the CW laser when the PV cell temperature is high enough.

The calculated time histories of the relative temperature change ($\Delta T/T_0$) of the PV cells illuminated by the laser with different *PPP* are compared with the experimental results as shown in Fig. 5(d), which indicate that the relative error is less than 10%.

It is verified theoretically that the temperature increment in the PV cell illuminated by the MP laser is always lower than that by the CW laser under the present conditions, which is ensured by the fact that the thermal dissipation percentage is lower in the PV cell illuminated by the MP laser as shown in Fig. 5(c). Therefore, a higher percentage of the MP laser in the hybrid laser applied to illuminate the PV cell would improve the overall light-electricity conversion efficiency and result in less thermal dissipation, which would reduce the temperature elevation of the cell in return. That might be the very reason why the maximum permitted laser power density was increased with increasing *PPP* for the present parameter range.

4. CONCLUSION

The multi-physical behaviors of multi-junction GaAs PV cells illuminated by the combined CW laser and MP laser were studied, and the failure criterion was defined on the cell material, by which the critical value of the average power density is found to fall into the range of 53 kW/m^2 and 150 kW/m^2 when the mixture degree *PPP* changes from 1 to 0. The theoretical results from the coupled model on the carrier transportation and thermal diffusion reveal that more thermal dissipation would rise in the PV cell illuminated by the CW laser than the MP laser, and of which the latter leads to smaller temperature elevation and, therefore, higher capacity in light-electricity conversion. This explains why the laser illumination with higher *PPP* value leads to a higher carrier collection rate and lower PV cell temperature rise effect under the present conditions.

Funding. Strategic Priority Research Program of Chinese Academy of Sciences (XDA17030100, XDA17030200); National Natural Science Foundation of China (11572327).

Disclosures. The authors declare no conflicts of interest.

Data availability. Data underlying the results presented in this paper may be obtained from the authors upon reasonable request.

REFERENCES

1. K. Jin and W. Zhou, "Wireless laser power transmission: a review of recent progress," IEEE Trans. Power Electron. **34**, 3842–3859 (2019).
2. C. W. Wu, R. T. Chang, and C. G. Huang, "Transient coupled model on efficiency prediction of laser power beaming for aerostat," Opt. Laser Technol. **127**, 106140 (2020).
3. B. E. Chertok, R. A. Evdokimov, V. P. Legostaev, V. A. Lopota, B. A. Sokolov, and V. Y. Tugaenko, "Remote electric power transfer between spacecrafts by infrared beamed energy," AIP Conf. Proc. **1402**, 489–496 (2011).
4. Y. Rathod and L. Hughes, "Simulating the charging of electric vehicles by laser," Proc. Comput. Sci. **155**, 527–534 (2019).
5. C. Soumya, B. Deepanraj, and J. Ranjitha, "A review on solar photovoltaic systems and its application in electricity generation," AIP Conf. Proc. **2396**, 020011 (2021).
6. J.-K. Sheu, F.-W. Huang, C.-H. Lee, M.-L. Lee, Y.-H. Yeh, P.-C. Chen, and W.-C. Lai, "Improved conversion efficiency of GaN-based solar cells with Mn-doped absorption layer," Appl. Phys. Lett. **103**, 063906 (2013).
7. A. De Vos and H. Pauwels, "On the thermodynamic limit of photovoltaic energy conversion," Appl. Phys. **25**, 119–125 (1981).

8. C. W. Wu, J. Wang, and C. G. Huang, “A coupled model on energy conversion in laser power beaming,” J. Power Sources **393**, 211–216 (2018).
9. T. Markvart, “Thermodynamics of losses in photovoltaic conversion,” Appl. Phys. Lett. **91**, 064102 (2007).
10. O. Höhn, A. W. Walker, A. W. Bett, and H. Helmers, “Optimal laser wavelength for efficient laser power converter operation over temperature,” Appl. Phys. Lett. **108**, 241104 (2016).
11. H. Helmers, E. Lopez, O. Höhn, D. Lackner, J. Schön, M. Schauerte, M. Schachtner, F. Dimroth, and A. W. Bett, “68.9% efficient GaAs-based photonic power conversion enabled by photon recycling and optical resonance,” Phys. Status Solidi RRL **15**, 2100113 (2021).
12. Y. C. Yuan and C. W. Wu, “Thermal analysis of film photovoltaic cell subjected to dual laser beam irradiation,” Appl. Therm. Eng. **88**, 410–417 (2015).
13. M. A. Shannon, B. Rubinsky, and R. E. Russo, “Mechanical stress power measurements during high-power laser ablation,” J. Appl. Phys. **80**, 4665–4672 (1996).
14. M. Takihara, T. Takahashi, and T. Ujihara, “Minority carrier lifetime in polycrystalline silicon solar cells studied by photoassisted Kelvin probe force microscopy,” Appl. Phys. Lett. **93**, 021902 (2008).
15. D. Xia and J. J. Krich, “Efficiency increase in multijunction monochromatic photovoltaic devices due to luminescent coupling,” J. Appl. Phys. **128**, 013101 (2020).
16. M. Mundusa, J. A. Giesecke, P. Fischer, J. Hohl-Ebinger, and W. Warta, “Interaction of ultrashort laser pulses and silicon solar cells under short circuit conditions,” J. Appl. Phys. **117**, 085702 (2015).
17. R. Khare, P. Shukla, G. Mishra, C. Mukherjee, S. Talwar, V. Dubey, P. Saxena, and J. Mittal, “A novel confocal optical pulse stretcher for laser pulses,” Opt. Commun. **282**, 3850–3853 (2009).
18. R. T. Chang, C. Liu, C. G. Huang, and C. W. Wu, “Responses of typical photovoltaic cell to dual laser irradiation,” in *3rd Optical Wireless and Fiber Power Transmission Conference* (2021).
19. S. Fafard and D. P. Masson, “Perspective on photovoltaic optical power converters,” J. Appl. Phys. **130**, 160901 (2021).
20. S. M. Sze, Y. Li, and K. K. Ng, *Physics of Semiconductor Devices* (Wiley, 2006).
21. F. P. Incropera and D. P. Witt, *Fundamentals of Heat and Mass Transfer* (Wiley, 2007).